Enhanced Photoluminescence at λ = 1.54 μm in the Cu-Doped Er:SiO 2 System

ARTICLE *in* THE JOURNAL OF PHYSICAL CHEMISTRY C · OCTOBER 2012

Impact Factor: 4.77 · DOI: 10.1021/jp306487a

6 AUTHORS, INCLUDING:

E. Cattaruzza
Università Ca' Foscari Venezia
137 PUBLICATIONS **2,098** CITATIONS
SEE PROFILE

Enrico Trave
Università Ca' Foscari Venezia
63 PUBLICATIONS **493** CITATIONS
SEE PROFILE

Giuliana Aquilanti
Sincrotrone Trieste S.C.p.A.
124 PUBLICATIONS **1,203** CITATIONS
SEE PROFILE

Gino Mariotto
University of Verona
273 PUBLICATIONS **3,253** CITATIONS
SEE PROFILE

THE JOURNAL OF PHYSICAL CHEMISTRY C

Article

pubs.acs.org/JPCC

Enhanced Photoluminescence at $\lambda = 1.54\ \mu m$ in the Cu-Doped Er:SiO_2 System

Elti Cattaruzza,*[,†] Giancarlo Battaglin,[†] Francesca Visentin,[†] Enrico Trave,[†] Giuliana Aquilanti,[‡] and Gino Mariotto[§]

[†]Molecular Sciences and Nanosystems Department, Università Ca' Foscari Venezia, via Torino 155/b, I-30172 Venezia-Mestre, Italy

[‡]Elettra-Sincrotrone Trieste S.C.p.A., s.s. 14 km 163.5, I-34149 Basovizza, Trieste, Italy

[§]Department of Computer Science, Università di Verona, Strada le Grazie 15, I-37134 Verona, Italy

ABSTRACT: The radiofrequency magnetron sputtering codeposition is a versatile technique to obtain Er-doped glass films, i.e., optical materials characterized by the emission of an intense photoluminescence signal at $\lambda = 1.54\ \mu m$, the most exploited wavelength for optical telecommunications through fiberglass. After the optimization of this radiative emission in the Er:SiO_2 systems, strong sensitizing effects in Cu-doped Er:SiO_2 glass systems were evidenced and investigated. Experimental findings suggested that the main energy-transfer mechanism in the metal-doped Er:SiO_2 system could be related only to the very small size (less than 1−2 nm) of the doping aggregates and not dependent on their composition.

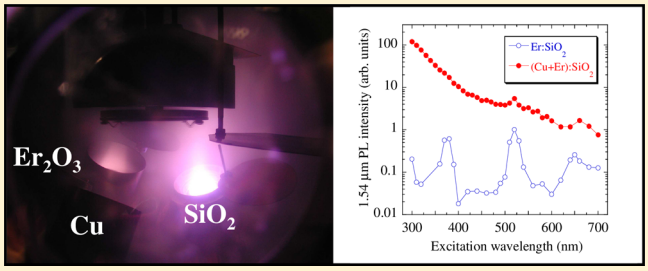

INTRODUCTION

Erbium-doped dielectric materials are used in the optical communication technology as active elements in photonic devices, with the Er^{3+} ions transition at 1.54 μm falling in the range of minimum transmission loss for silica optical fibers.[1] Planar integrated optical devices, in which all of the optical components are fabricated and directly integrated on a single chip, are needed to built an all-optical communication network.[2] Planar photonic integrated circuits can perform functions such as guiding, splitting, switching, wavelength multiplexing, and amplification of light. In many cases silicon is used as a substrate, thus allowing optoelectronic integration with other devices. If embedded in pure silica, erbium ions exhibit only resonant excitation, with a very small excitation cross-section. An increase of the excitation is possible in Er:silica systems by doping with other rare-earth metals[3,4] or elements such as Si,[5−7] Ag,[8−10] Au[11−13] mainly in the form of very small aggregates and/or nanoclusters: the dopant atoms act as sensitizers of erbium luminescence allowing broad band excitation at wavelengths not absorbed by erbium, with an effective increase of the excitation cross-section.[14] As a matter of fact, subnanometric aggregates made of few atoms seem to be the best ones for the sensitization of the rare-earth by Au and Ag metals,[8−13] even if the mechanisms of energy-transfer between the sensitizing atoms and the rare-earth is still not completely understood.

In spite of the usually used sensitizers-acting metals, we decided to choose an up-to-now uninvestigated metal, copper, that belongs to the same group of Ag and Au in the periodic table. As a matter of fact, in the bulk phase the noble metals show luminescence properties related to very similar excitation and recombination mechanisms, involving a band structure which include an s−p conduction band and two sets of d bands.[15,16] In the case of Cu, for excitation energies lower than ∼3 eV, the luminescence spectrum consists of a single peak, centered at ∼570 nm; this main signal is strongly enhanced in bulk metallic copper with a rough surface, due to localized plasmon resonances.[15,16] The same local-field enhancement happens in the case of Cu (nano)particles, due to the coupling of incoming and outgoing fields to the local surface plasma oscillation,[17] and this effect is more marked when the contribution of the surface is dominant, i.e., for very small particles. The well-known luminescent activity of the noble metal nanoparticles [ref 17 and references therein] as well as of the copper ions [refs 18 and references therein] suggests that copper could be an interesting sensitizing metal for erbium too.

For the preparation of the samples, we used a deposition route to easily synthesize optically active Er:SiO_2 films doped with, in principle, any sensitizing metals: this was possible by our multisource radiofrequency (RF) magnetron sputtering deposition apparatus, allowing energetic treatments during the growth of the film too. Energetic treatments during the sputtering deposition, like thermal heating and/or RF (or DC) bias, give rise to different microstructures of the growing film, in agreement with structure-zone models[19] that relate the microstructure and the most prominent deposition parameters. The different microstructures obtained by changing the deposition parameters lead to final film configurations that

Received: July 1, 2012
Revised: September 5, 2012
Published: September 6, 2012

   dx.doi.org/10.1021/jp306487a | J. Phys. Chem. C 2012, 116, 21001−21011

can remain different also after subsequent thermal annealing. A RF power applied to the sample holder can modify the overall plasma configuration inducing an oscillating RF voltage of negative mean value on the sample itself. This gives rise to a low-energy bombardment of the growing structure by the ions coming from the plasma (the same happens by using a negative DC bias).

In a recent work concerning the optimization of the 1.54 μm radiative emission in Er-doped stoichiometric SiO_2 films made by sputtering systems,[20] we explored all of these degrees of freedom, finding that proper RF bias and heating conditions allow for the synthesis of thin films with luminescence properties comparable to systems realized by other synthesis routes, like ion implantation and sol−gel method. Moreover, as a clear indication of the efficiency of the energetic "assistance" during the deposition, it is worth noting that Er-doped films synthesized without any energetic assistance during the deposition show a modest PL activity, even after proper postsynthesis annealing. Taking inspiration from this work, we synthesized three different (Er+Cu):SiO_2 films with sputtering deposition assisted by sample bias, sample heating, or both of these energetic treatments.

EXPERIMENTAL METHODS

(Er+Cu) codoped silica films were synthesized by simultaneous deposition of copper, erbia, and silica on fused silica slides 25 × 75 mm^2, 1 mm thick, in a custom-built radiofrequency magnetron sputtering deposition apparatus. Codepositions were performed by means of three 13.56 MHz radiofrequency sources acting in a neutral atmosphere (pure Ar), at a pressure of 40×10^{-2} Pa. The magnetron sources were tilted offline to adjust the deposition focal point on the silica substrates. During depositions, the sample holder was rotated at 5 rpm to have a good homogeneity of the film composition and thickness. The RF power to the 2 in. diameter targets was fixed at 4, 12, and 150 W for copper, erbia, and silica, respectively. After a four-step cleaning in ultrasonic bath (deionized H_2O, trichloroethylene, acetone, and isopropyl alcohol), immediately before the deposition the silica slide substrates were RF-biased at 20 W for 20 min to remove possible surface contaminations and to chemically activate the surface. The thickness of the removed layer was estimated to be about 10 nm. The 75 min codeposition of copper, erbia, and silica was followed by a single silica deposition for 15 min to have a capping protective layer. The thickness of the whole deposited film was around 350 nm. Three different synthesis routes were explored, i.e., sputtering deposition assisted by (i) −50 V RF bias, (ii) 500 °C heating, and (iii) both energetic treatments. Immediately after the synthesis the samples were put in a drybox and kept at a pressure around 1 Pa until a final thermal annealing. The annealing treatment (always for 1 h in air) was done at constant temperature T, in the range 200−800 °C. In the following, we refer to the final samples by labels such as "Cu(50−500)800", meaning that the (Er+Cu):SiO_2 thin film was deposited with 50 V of negative bias and at 500 °C of temperature, with a postdeposition annealing at 800 °C.

Composition of the samples and concentration profiles of the different elements were obtained by Rutherford backscattering spectrometry (RBS) measurements, performed at Laboratori Nazionali INFN-Legnaro, Italy by using a $^4He^+$ beam at the energy of 2.0 MeV, with the detector placed at 160° with respect to the incident beam direction.

Optical absorption characterization has been performed with a JASCO V670 spectrophotometer in the 200−900 nm wavelength range. Er ions photoluminescence (PL) investigation was carried out by exciting the sample with a cw Ar laser, whose pumping lines at 488 and 476.5 nm allow for rare-earth photostimulation in resonance (matching the transition between the Er^{3+} ion $^4I_{15/2}$ ground state and the $^4F_{7/2}$ excited level) and in out-of-resonance conditions (pumping radiation not directly absorbed by the rare-earth), respectively. The laser beam had a spot diameter of about 1 mm and it was modulated by a mechanical chopper. A single-grating monochromator provided the spectral discrimination of the luminescence signal, which was detected by a N_2-cooled photomultiplier tube operating in the 1000−1650 nm spectral range. PL emission was acquired with a lock-in amplifier, using the chopper frequency as reference. Time-resolved PL analysis was carried out by fixing the detected wavelength and collecting the PL intensity evolution as a function of the time with a transient digitizer (overall time resolution of about 5 μs). PL excitation (PLE) measurements were performed by pumping the samples through a Xe lamp coupled to a monochromator, scanned in the 250−800 nm wavelength range.

X-ray absorption spectroscopy (XAS) experiments were performed at Elettra Laboratory, in Basovizza, Trieste (Italy), at the XAFS beamline.[21] The storage ring operated at 2.0 GeV in top-up mode with a typical current of 300 mA. The Cu K-edge of the different samples was recorded at room temperature in fluorescence mode, using a large area Si drift diode detector (KETEK GmbH AXAS-M). Samples of Cu, Cu_2O and CuO were also measured as references of metallic and oxidized copper in transmission mode. The energies were defined by assigning the first inflection point of the spectra of the metallic copper to 8979.0 eV. The monochromator was equipped with a couple of Si(111) crystals, and the harmonic rejection was achieved by detuning the second crystal of the monochromator by 30% of the maximum. A reference sample of metallic copper was used for energy calibration in each scan. This allowed us a continuous monitoring of the energy during consecutive scans.

Polarized micro-Raman spectra were carried out at room temperature in backscattering geometry using a triple-axis monochromator (Horiba-Jobin Yvon, model T64000), set in double-subtractive/single configuration and equipped with holographic gratings having 1800 lines/mm. The spectra were excited at some wavelengths by a mixed Ar−Kr ion gas laser, but only the 568.2 nm line allowed for a suitable detection of the Raman spectrum of both the glass matrix and the embedded Cu clusters. In fact, for this excitation line two crucial conditions were simultaneously fulfilled; that is, first, the emission line of the Er^{3+} ion turns out to fall far away from the laser line, and second, it ensures the nearly resonant match with the Cu plasmon energy, in order to obtain an important enhancement of Raman scattering from acoustic vibrations of Cu clusters. The laser beam was focused onto the main surface of sample over a region of about 1 μm in size through the lens of a 100X microscope objective and the scattered radiation from this region was collected in confocal mode throughout the same objective. By means of this approach, about 1 μm thickness was probed from the surface. The low-frequency Raman were carried out keeping the power on the sample surface at 3.5 mW. The scattered radiation, filtered by the double-monochromator, was detected by a CCD detector cooled by liquid nitrogen at approximately −130 °C. The spectrometer resolution was better than 0.6 cm^{-1}/pixel. In

dx.doi.org/10.1021/jp306487a | J. Phys. Chem. C 2012, 116, 21001−21011

order to accurately determine the peak wavenumber of observed Raman bands, some emission sharp lines originating either from secondary emission of plasma or from a calibrated neon lamp were used as reference. Repeated micro-Raman measurements on different sample microregions were run under the same experimental conditions, and the recorded spectra exhibited a very good reproducibility. The recorded spectra were processed to remove artifacts due to cosmic rays, whereas the luminescence background observed in some samples and consisting of a nearly flat and structureless line of appreciable intensity, underlying the Raman spectrum, was subtracted before the data analysis.

RESULTS

After deposition, the samples were kept in vacuum-dry conditions because samples left in air for a long time before the final annealing did not show detectable photoluminescence signals even after annealing: in fact, ambient moisture can cause a "poisoning" of the film, and the subsequent annealing results in a final silica film structure with many stable defects involving OH groups. Hydroxyl impurities are one of the important quenching centers in Er-doped glasses: the 1.54 μm Er^{3+} transition corresponds to the energy of the second harmonic of the OH stretching vibration.[22] If an Er^{3+} ion is coupled to an OH, nonradiative relaxation can take place.

As commonly observed for the Er:SiO_2 system synthesized by different techniques, full Er ion luminescence activation can be achieved by suitable postsynthesis heating at high temperature, like 800 °C as stated in ref 20 for our sputtered films. In fact, it is well-known that this kind of treatment is useful to anneal the structural defects in the as-deposited Er:SiO_2 film,[20,23,24] which can act as nonradiative centers for Er ion relaxation with consequent reduction of the 1.54 μm emission efficiency.

a. Compositional Analysis. The (Er+Cu) codoped silica samples were synthesized with compositions in the range (1.1−2.4) × 10^{20} atoms/cm^3 and (5.4−8.5) × 10^{20} atoms/cm^3 for erbium and copper, respectively (as determined by RBS), depending on the deposition parameters. The total amount of dopant atoms inside the silica film was around 5 × 10^{15} Er/cm^2 and 25 × 10^{15} Cu/cm^2. The reduced doping level for both erbium and copper (≤1 at. %) was chosen for (i) preventing luminescence quenching effects due to cooperative nonradiative de-excitation between rare-earth ions and (ii) controlling the evolution of the early stage of Cu clustering before massive metal precipitation, with the aim of studying its influence on the glass optical properties as a function of postsynthesis thermal treatments at different temperature.

For all of the samples, the detected O/Si ratio by RBS was in the range 2.00−2.25: this excludes the formation of Si aggregates as a consequence of the final annealing. RBS measurements showed also that the in-depth concentrations of Cu and Er were nearly constant in the doped film. They did not vary after the postsynthesis annealing: neither copper nor erbium segregation regions were detected. Depending on the energetic treatment performed during the synthesis, different amounts of Ar were trapped inside the film: the highest value (about 1.6 × 10^{21} atoms/cm^3) was reached in the biased samples, i.e., the samples subjected to a low-energy Ar^+ bombardment during their growth. The trapped Ar amount decreases after the final annealing: in particular, after 1 h in air at 800 °C it is near the RBS detection limit in all of the samples (corresponding to about 1 × 10^{20} atoms/cm^3).

b. Optical Absorption Analysis. The presence of noble metal nanoparticles in a dielectric matrix can be easily revealed and monitored by means of optical absorption measurements: indeed, the collective motion of the free electrons inside the (nano)particle under optical stimulation gives rise to a characteristics absorption band called surface plasmon resonance (SPR).[25] To get information on the copper nanoparticles formation and on their size, we performed on all samples an optical absorption investigation, and we simulated the obtained spectrum by means of the Mie classical approach applied to a composite glass system made by copper metal nanospheres embedded in silica, namely considering the dielectric function of the copper particles having a Drude-like contribution due to the conduction electrons and taking into account the dependence of the dielectric function on the particle dimension. We consider only the dipolar absorption. The size-dependence is phenomenologically introduced by taking into account the so-called surface scattering-limited mean-free-path effect through a size-dependent electron scattering rate S of the form $S_{rate}(R) = S_{rate}(\infty) + Av_F/R$, where v_F is the Fermi velocity, R is the particle radius, and A is a model-dependent parameter:[25−31] with this approach it is possible to ensure the broadening and damping of the surface plasmon resonance characteristics of small particles, as explained below. This method is valid for composites with metal particle filling factor $p \ll 1$ and particle radius $R \ll \lambda$, where λ is the wavelength of light used. In our samples, supposing that all of the embedded copper forms metal particles, we obtain a maximum value of the filling factor $p_{max} = 0.01$; thus, the Mie approach is justified (for particle radii up to a few tens of nm). We used the copper dielectric function calculated from the optical constants obtained by Johnson and Christy;[32] with the optical constants of the Ioffe Physical-Technical Institute database,[33] we had very similar results. We assumed for simplicity a monodimensional size distribution of spherical particles.

The peculiarity of Cu nanoparticles if compared to Ag and Au ones is the dramatic damping of the SPR band with decreasing particle size. Indeed, for Cu nanoparticles embedded in silica, the surface plasmon resonance lies around 2.2 eV (560 nm of wavelength), i.e., in the region of interband transitions, corresponding to electronic excitations from full 3d-valence electron bands located just below the Fermi energy to unoccupied electron levels above the Fermi energy (the interband transitions threshold is about 1.9 eV).[27,34] This means that for copper particle radii smaller than, we say, 1 nm, i.e., for particles of less than few hundreds of atoms, it is nearly impossible to detect the SPR band in the optical absorption spectrum.

In general, different temperatures of the final annealing are able to induce different behaviors from the copper, in terms of chemical bonds, diffusion, and/or precipitation.[31,35] In Figure 1 the optical absorption spectra of the Cu(50−500) group samples, i.e., those prepared with both energetic treatments during the synthesis, are shown. An absorption band with its maximum around 560 nm is recognizable for the samples annealed at temperature higher than 600 °C. On the basis of the wavelength of the maximum, this band is attributed to the SPR of copper metal nanoparticles embedded in silica matrix.[25] Little important features are visible in the spectra of Figure 1, such as some absorbance oscillations due to multiple reflection effects: from their estimated wavelength position one can roughly predict the thickness of the film, obtaining evaluations in agreement both with measurements done by a profilometer

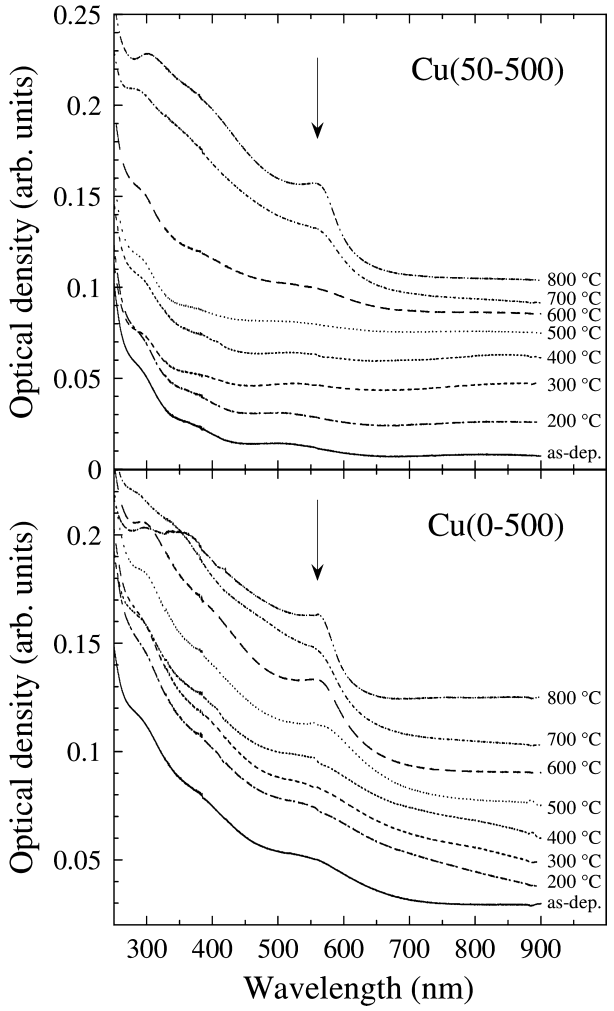

Figure 1. Optical absorption spectra of Cu(50−500) and Cu(0−500) samples before and after 1 h thermal annealing in air, in the 200−800 °C range. The arrow shows the position of the surface plasmon resonance (SPR) band.

and calculations starting from the RBS findings. The spectra related to thermal annealing up to 500 °C are similar in shape but they show an increase of the absorption for wavelengths smaller than 450 nm (energies larger than 2.7 eV). This is mainly due to the rising of the interband transitions as the copper aggregates start to form and their size increases. The absence of the SPR band suggests that the Cu particles possibly present are smaller than 1−2 nm in size. At T > 600 °C the appearance of the clearly visible SPR band, together with the strong edge increase of the interband transition, testifies to the formation of larger Cu nanoparticles: simulations gave a mean size of 2 ± 1 nm for the 700 °C sample and 3 ± 1 nm for the 800 °C sample. The samples of the Cu(50-RT) group show very similar characteristics (spectra not reported).

The behavior of the absorption spectra of the Cu(0−500) group samples is different (Figure 1). First of all, the samples exhibit a more marked absorption in the region near UV; moreover, the SPR band starts to be visible from lower annealing temperature (500 °C). These experimental findings suggest that very small copper aggregates could be already present before the postdeposition annealing, with a consequent relevant growth of the particle mean size for relatively low annealing temperature.

c. Photoluminescence Analyses (In- and Out-Resonance). The described materials revealed remarkable photoluminescence optical properties. In Figure 2 we report the

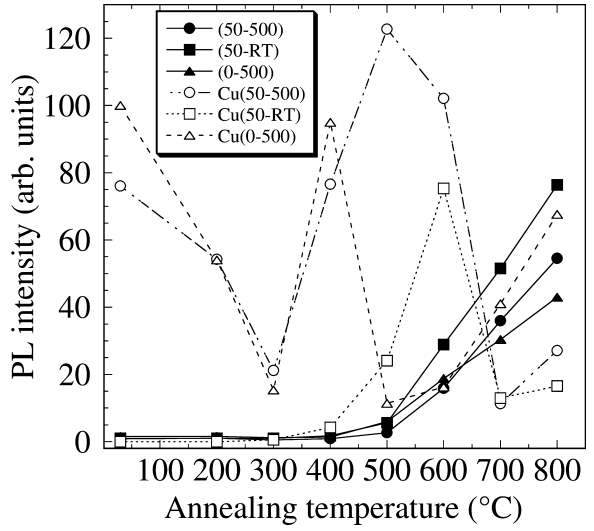

Figure 2. Photoluminescence emission intensity I measured at λ = 1.54 μm for the three (Cu+Er):SiO_2 systems (empty markers), compared to the equivalent "pure" Er:SiO_2 ones (filled markers), as a function of the temperature of the postsynthesis annealing (1 h in air). λ_{exc} = 488.0 nm. P = 25 mW. All lines are a guide to the eye. Relative uncertainties are below 10%.

photoluminescence emission intensity at 1.54 μm recorded for all the samples of the three groups, together with the corresponding samples synthesized without copper (Er:SiO_2 samples). The intensity of any sample was always divided by the total amount of erbium in that particular sample (as evaluated by RBS), thus allowing to rightly compare the signals of different samples. The measurements in Figure 2 were done by pumping in resonance condition (λ = 488.0 nm). The fwhm of the 1.54 μm PL signal is 33 nm in the Cu-doped samples, similar to the fwhm found in the undoped ones (30 nm). The "pure" Er:SiO_2 samples do not show PL emission before the final annealing; a detectable normalized intensity signal, increasing with the annealing temperature, is visible only for annealing between 500 and 800 °C. This behavior is mainly related to an increase of the quantum efficiency (i.e., an increase of the decay time) and, to a less degree, of the fraction of optically active Er ions[20] (a right local order around the erbium ions, in term of both number and distance of the first-neighbor oxygen atoms, is needed for optimizing the optical emission properties).[23] The best thermal treatments temperature is 800 °C, for which the silica significantly reduces the concentration of all its main defects[36] thus lowering the probability of nonradiative decay of the excited Er ions. At higher temperatures[20,24] we detected a decrease of the intensity, probably related to erbium clustering effects inducing local concentration quenching with reduction of the fraction of optically active ions,[37] even if in the case of rapid thermal annealing (RTA) in Er−Si−O/Si multilayer systems a high temperature treatment has been observed to increase the PL intensity.[38]

The photoluminescence emission of the (Er+Cu):SiO_2 samples shows several interesting features. At resonance, the presence of the copper atoms allows a marked PL signals in the as-deposited samples if synthesized with 500 °C substrate

dx.doi.org/10.1021/jp306487a | J. Phys. Chem. C 2012, 116, 21001−21011

heating (Figure 2). For these two sample groups, i.e., Cu(50−500) and Cu(0−500), by increasing the postdeposition annealing temperature, the PL intensity first decreases and then increases showing a maximum: this very high value of the PL intensity is detected for temperatures that depend on the sample group. The intensity falls for annealing at the highest temperatures, but in all three groups there is at least one sample (i.e., one annealing temperature) for which the value of the PL intensity is higher than that detected in the equivalent undoped system, indicating the effectiveness of the Cu doping as a way to increase the PL emission by resonant pumping. By the comparison with the experimental findings obtained by the optical absorption measurements in Figure 1, we can relate the presence and the dimension of copper aggregates to the occurrence of an indirect excitation channel for Er ions, an energy transfer. For the Cu(50−500) group, the best-performing one, the absorption spectroscopy showed the presence of the SPR band (that is of copper nanoparticles larger than 1−2 nm in size) only in the samples annealed at temperatures as high as 600 °C: starting at this temperature the decrease of the PL intensity, we deduce that copper clusters larger than a few nm do not favor the energy-transfer to the erbium ions, having instead a detrimental effect on the photoluminescence properties. The strong energy-transfer process between copper nanoparticles (and/or multimers) and erbium ions was verified by changing the Ar^+ laser excitation wavelength from 488.0 nm (in resonance with the $^4F_{7/2}$ level of Er, thus allowing a direct excitation) to 476.5 nm (which is nonresonant with any Er^{3+} energy levels). In Figure 3

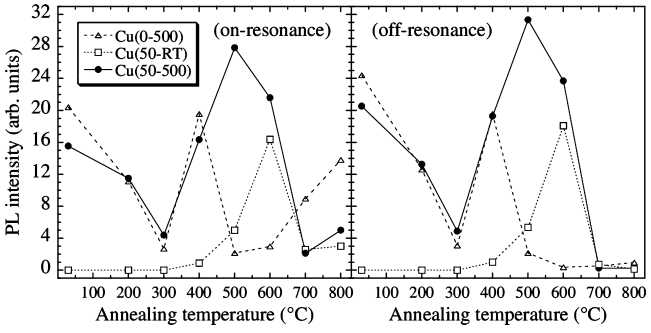

Figure 3. Photoluminescence emission intensity I measured at λ = 1.54 μm for the three (Cu+Er):SiO_2 systems, as a function of the temperature of the postsynthesis annealing (1 h in air). On-resonance: λ_{exc} = 488.0 nm; off-resonance: λ_{exc} = 476.5 nm. P = 6 mw. All lines are a guide to the eye. Relative uncertainties are below 10%.

the PL normalized intensity is reported for the three Cu-doped sample groups, obtained by on- and off-resonance pumping, respectively, with the same value of the pump power. A relevant PL signal at 1540 nm was observed also under 476.5 nm pumping, demonstrating that an important contribution to the Er luminescence takes place due to energy-transfer processes from the Cu structures to Er ions. Actually, no PL signals are observed by pumping nonresonantly the equivalent samples not containing copper. Data in Figure 3 show that the off-resonance PL intensity is very similar to the on-resonance one, indicating a very strong coupling between erbium ions and the copper structures responsible for the sensitization: this means that the copper-mediated excitation process of the rare-earth is predominant on the direct rare-earth light absorption. The presence of strong PL signals in the as-deposited sample at 500 °C, i.e., before the final annealing, could be due to energy-transfer from very small copper aggregates and/or multimers, already formed inside the matrix because of thermal effects during the film growth that favor diffusion and aggregation of Cu atoms. This indicates that the sensitization effect is active without further recovery of the matrix.

Time resolved PL analysis reveals that the Cu-doped samples are characterized by nonexponential decay for the Er emission at 1.54 μm (Figure 4). On the other hand, the equivalent

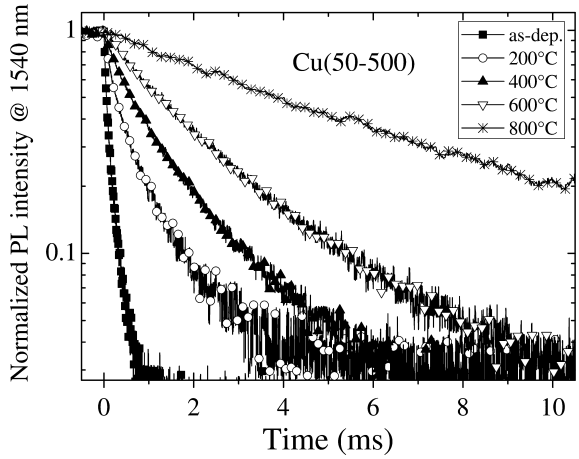

Figure 4. PL time decay curves measured at λ = 1.54 μm from the series of samples Cu(50−500) as-deposited and after 1 h annealing in air, in the 200−800 °C temperature range. Only a selection of curves is reported for clarity. Ar laser excitation parameters: λ_{exc} = 488.0 nm, P = 25 mW. The Y axis is plotted in logarithmic units for highlighting the nonexponential trend of the lifetime curves.

undoped samples exhibit lifetime curves with single exponential behavior. We argue that the presence of copper can locally influence the PL dynamics for each single Er ion causing such a spread on the spontaneous lifetime values for the $^4I_{13/2}$ state. This can be due to local changes of the refractive index induced by copper concentration variation, or to the opening of further nonradiative de-excitation channels in the heterogeneous medium, with consequent lifetime reduction as the emitting Er ion gets closer to the interacting codoping species.[39,40]

Considering the multiexponential form of the recorded PL decay signals, we decided to fit the curves with a stretched-exponential function of the form

$$I_{PL}(t) = I_{PL}(0)\exp\left[-\left(\frac{t}{\tau}\right)^{\beta}\right] \quad (1)$$

where τ is the spontaneous lifetime characterizing the Er ion population and β is the stretching factor which accounts for the lifetime dispersion and varies between 0 and 1, approaching the upper limit when the decay curve is more and more characterized by the single-exponential behavior. The calculated lifetime values increase with the annealing temperature, starting from 0.4 ms for the as-deposited samples and increasing monotonically up to nearly 6 ms in the case of the 800 °C treatment (a value smaller than for the undoped samples, around 8 ms). A similar behavior is observed for the β parameter that starts from 0.6 and increases to 1 for the annealing at the highest temperature, being the curves practically of the single-exponential form.

dx.doi.org/10.1021/jp306487a | J. Phys. Chem. C 2012, 116, 21001−21011

d. Structural Analyses: X-ray Absorption Spectroscopy (XAS). We decided to deeply analyze the structure of the samples of the series Cu(50−500), the best-performing one from the luminescence point of view. An X-ray diffraction analysis made with a commercial diffractometer was not able to show features related to the presence of copper nanoparticles. This is an expected result, because the samples were extremely diluted and had possible copper nanoparticle sizes less than a few nm. We were then forced to use a synchrotron radiation technique such as XAS. The following four samples were analyzed.

1. Cu(50−500)as-dep: it is the sample with no thermal treatment after deposition, i.e. the "starting point" of the series; this sample shows a good luminescence activity.
2. Cu(50−500)300: after the 300 °C thermal treatment, the luminescence activity is quite completely absent.
3. Cu(50−500)500: after the 500 °C thermal treatment, the luminescence activity increases and reaches its maximum value.
4. Cu(50−500)800: after the 800 °C thermal treatment, the luminescence activity is suppressed. As shown by the optical absorption analysis, copper precipitates in the nm range of size are certainly present inside this sample.

For the sake of clarity, in this paragraph these four samples are called below simply "as-dep", "300 °C", "500 °C", and "800 °C". Figure 5 shows the normalized absorption of the samples, together with the reference ones (Cu, CuO, and Cu_2O).

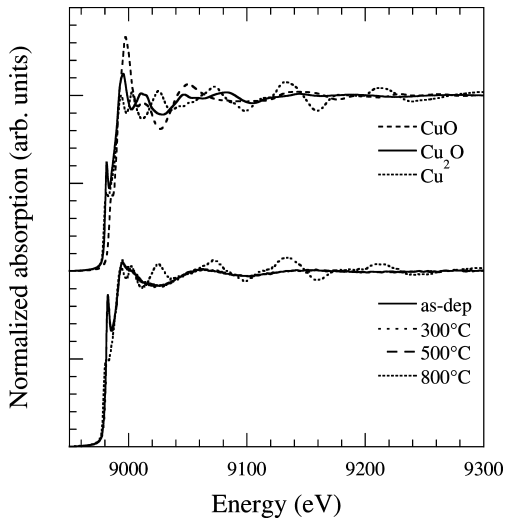

Figure 5. Cu K-edge normalized absorption spectra of samples as-dep, 300 °C, 500 °C, and 800 °C of the series Cu(50−500), together with those of the reference samples CuO, Cu_2O, and Cu.

As far as the 800 °C sample is concerned, the frequency of its oscillations in Figure 5 is the same as those of the metallic copper, although the amplitude is largely reduced: this result evidences the presence of a large amount of copper in the metallic state, in agreement with the optical absorption analysis. Almost all of the copper atoms inside this sample are forming metallic precipitates; the reduced amplitude of the oscillations may be related to a small size of the metallic copper structures, as discussed below.

Instead, the absorption edges shown by the samples as-dep, 300 °C, and 500 °C are characterized by the same features but completely different from the sample 800 °C. The onset of the absorption edge for the spectra of the first three samples evidences the presence of a strong prepeak, characteristic of Cu^+: this means that in these samples almost all of the copper atoms are in a +1 oxidation state. If present, metallic copper is less than a few percent of the total Cu amount. A closer look at the edge region shows that the onset of absorption of sample 300 °C is shifted toward higher energy with respect to the other two samples, namely toward the energies characteristics of oxidized copper. The shift is ∼0.4 eV. This is a small but detectable difference, which may suggest, in a qualitative way, the possibility of a copper behavior slightly more "metallic" for the samples as-dep and 500 °C than that for 300 °C.

In Figure 6a the modulus of the Fourier transform (FT) is shown for the three samples and the Cu_2O standard. The first peak of the FT of the three samples corresponds to that of Cu_2O. This means that the local coordination of Cu is very similar to that of cuprite (for which the first coordination shell is formed by two oxygen atoms at 1.849 Å). However, the second coordination shell given by 12 Cu atoms in Cu_2O is completely lost in our samples, suggesting that copper atoms are dispersed inside the silica network, forming chemical bonds with oxygen. Another interesting difference between the 300 °C and the other two samples is the position of the second peak, centered at a different value: this characteristic is not an artifact, being detectable also by changing the processing parameters. For samples as-dep and 500 °C the second small peak is at the same R value of the Cu−Cu coordination in metallic copper. This result is in agreement with what has been discussed for the onsets of absorption and may suggest the presence of a small amount of metallic copper in these two samples.

The sample 800 °C presents the same features of metallic copper, as evidenced in Figure 6b by the modulus of the FT. However, a reduction of the amplitude is evident, indicating a reduced size of the copper precipitates. A quantitative fit of the first shell has been done by using the structure of metallic copper as a model. During the fitting procedure the S_0^2, E_0, and σ^2 parameters have been kept fixed to the values found for bulk Cu, whereas the coordination number and the interatomic distance have been considered as free parameters. The coordination number CN found is 9.7(3) (for bulk Cu CN = 12): on the basis of the relationship between the degeneracy of the first shell of Pt (that in the bulk phase has the same structure of Cu) and the dimension of the particles,[41] the coordination number found for this sample corresponds to an average particle size of 2.5(2) nm. This is in good agreement with the size estimation obtained by the Mie simulation of the optical spectrum, as described above. In addition, a line profile analysis of the X-ray diffraction spectrum (not reported here) for the same 800 °C sample, obtained in grazing incident mode by using synchrotron radiation, gave a volumetric mean size of spherical particles of 2.6 nm, namely quite the same obtained by XAS analysis.

e. Vibrational Characterization: Low-Frequency Raman Spectroscopy. Raman spectroscopy in the very low-wavenumbers region has been proved to be one of the most outstanding nondestructive techniques to study the microstructure in low-dimensional systems composed of very small aggregates, such as nanoclusters and nanocrystals, dispersed in solid transparent dielectric matrices. In particular, this technique can give information on the average size of the nanoparticles, on their size distribution and, also, on the particle−matrix coupling or interaction. The occurrence of distinct peaks in the low-frequency region of Raman scattering

dx.doi.org/10.1021/jp306487a | J. Phys. Chem. C 2012, 116, 21001−21011

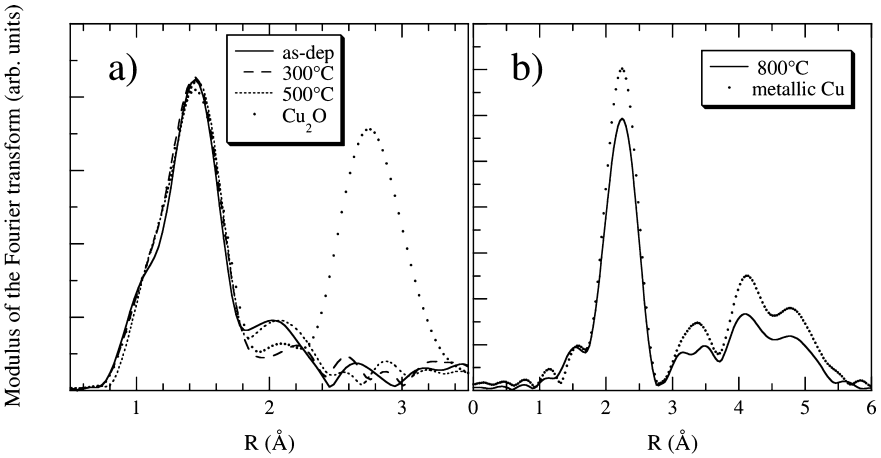

Figure 6. Modulus of the Fourier transform. (a) Samples as-dep, 300 °C, and 500 °C compared with cuprite standard; (b) sample 800 °C compared with metallic copper standard.

has been discussed in terms of acoustic-phonon modes confined in the homogeneous nanoparticle volume.[42−46] Previous studies, carried out either on transparent dielectric materials containing metal nanoclusters[44,47−50] or semiconductor quantum dots,[51−54] confirmed that low-frequency Raman scattering, below 100 cm^{-1}, is very sensitive to features with characteristic lengths from one to tens of nanometers.

The as-recorded anti-Stokes and Stokes-shifted in the low-wavenumber micro-Raman spectra, carried out from three Cu(50−500) samples (those annealed at the highest temperatures) in confocal mode at room temperature in crossed polarization, are shown in Figure 7. The spectra of the samples

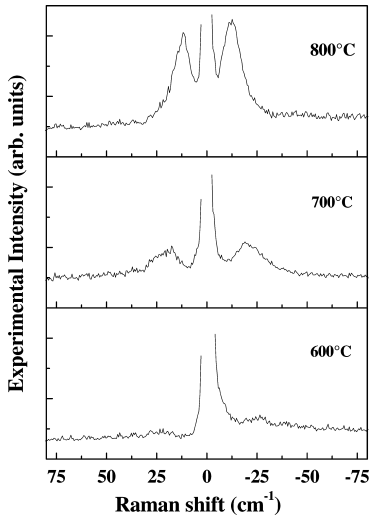

Figure 7. Typical low-frequency confocal micro-Raman spectra of three Cu(50−500) annealed samples, carried out in crossed (HV) polarization at room temperature, under excitation of the 568.2 nm laser line, matching the surface plasmon resonance. The annealing temperature is reported.

annealed at 800 and 700 °C clearly exhibit a well shaped band, although of quite unlike intensity, peaked at about 12 and 19 cm^{-1}, respectively. In contrast, only a weak, hardly observable, feature centered at about 25 cm^{-1} appears in the spectrum of the sample treated at 600 °C. This low-wavenumber band, not present in the low-frequency Raman spectrum of bare glass and of Cu-doped samples treated at lower temperatures, should be referred to the presence of copper nanoclusters within the host silica matrix. In fact, similar spectral features were observed in the low-wavenumber Raman scattering of silica glass containing spherical metal clusters, namely silver and copper nanoparticles,[44,47−50] and they were systematically attributed to the scattering from acoustic vibrational modes of metal nanoparticles. Therefore, the observed phenomenology suggests the occurrence of an appreciable Cu precipitation in clusters within the silica matrix starting from treatments at 600 °C, whereas this process becomes more and more relevant, as evidenced by spectral features like peak intensity, position and width, when the treatment temperature increases. As a matter of fact, the Raman spectra of Figure 7 show a broad band that increases in intensity and shifts toward lower frequencies upon increasing the annealing temperature, meanwhile its width decreases. Moreover, the shape of this band turns out the be independent of the polarization configuration, either parallel or crossed, so that, on the basis of well established experimental observations on the low frequency Raman scattering from nanoparticles embedded in dielectric matrices, this feature can be reasonable assigned to the fundamental spheroidal quadrupolar mode of the Cu aggregates precipitated within the glass matrix. Therefore, assuming the clusters as nanospheres, according to Duval et al.[42] the frequency ω of this nanoparticle mode depends on the nanoparticles size, following the equation:

$$\omega = AV_T/cD \quad (2)$$

where A is a proportionality coefficient, V_T is the transverse velocity of sound in copper, c is the velocity of light in vacuum, and D is the average diameter of the vibrating sphere. In the case of freely vibrating nanospheres the frequency of the fundamental quadrupolar mode is obtained assuming $A = 0.84$; obviously, the A value should be properly determined in the case of nanospheres embedded into dielectric matrices, taking into account both their elastic and density parameters. So, for instance, the value of this proportionality coefficient for metallic Cu nanoclusters incorporated in a soda-lime glass turns out to be 0.95.[49]

In our case, any reliable simulation of the main spectral parameters, characterizing the observed low-frequency Raman scattering from Cu clusters embedded in glass matrix, cannot be carried out due to a lack of data about the density and elastic properties of our sputtered silica films. In spite of this, the

dx.doi.org/10.1021/jp306487a | J. Phys. Chem. C 2012, 116, 21001−21011

observed behavior versus the annealing temperature of the particle peak, in terms of its intensity, position and width, clearly indicates the occurrence of a progressive increase of either the number of scattering centers, that is the particles density, or the diameter of Cu nanoclusters, that is the particles volume, with a concomitant relevant decrease of the particle size distribution, revealed by the narrowing of the Raman band. By the way, a rough evaluation of the mean nanoparticle size can be derived from the frequency position of the maximum of the acoustic peak, on the basis of the eq 2 reported above, under the approximation of freely vibrating spherical nanoclusters and assuming a V_T value of 2648 ms^{-1} for metal Cu.[48] Taking into account the uncertainties related to the determination of the proportional coefficient A and of the transverse sound velocity V_T (for instance, other values can be found in literature for V_T, such as 2260 ms^{-1}),[55] the mean nanoparticle diameter D calculated from the frequency position of the maximum of the acoustic peaks in the HV polarized Raman spectra of samples treated at 800 and 700 °C is found to be $D_{800°C} = (6 \pm 2)$ nm and $D_{700°C} = (4.1 \pm 1.5)$ nm, respectively. In the case of the sample treated at 600 °C, the very faint peak detected suggests a mean nanoparticle diameter $D_{600°C} = (2.8 \pm 1.0)$ nm. All these rough estimations are in agreement with the size determination obtained by XAS and optical absorption. The discrepancy between the average particle size derived from low-frequency particle peak, detected by Raman scattering, and the volumetric mean size of nanospheres measured by X-ray techniques is not unexpected, being related the to the different correlation lengths probed by the different techniques, particularly in presence of nonspherically shaped nanoparticles. Considering that the Raman intensity of the particle modes is proportional to the volume of the particles themselves, and taking into account that in the 800 °C sample all the copper is present in the form of metallic nanoparticles (as evidenced by the XAS measurements reported above), we can assert that in the 700 °C sample the fraction of copper forming metallic aggregates is about 40% of the total amount of copper, while in the 600 °C sample this fraction is as low as 10%.

In all other samples of the Cu(50−500) series, no peaks related to copper nanoparticles are detected, suggesting one or both of the following possibilities: (i) if present, the copper aggregates have mean size smaller than a threshold value, this last estimated to be around 2 nm and (ii) if present with mean size larger than the threshold value, the copper metallic aggregates concern a fraction of the total amount of copper lower than a threshold value (estimated to be around 2×10^{15} Cu/cm^2, i.e. of the order of the 10% of the total copper amount in our samples). The two threshold values are estimated considering the whole sensitivity of the experimental setup and the technique. However, the absence of any signal related to metallic copper aggregates in all the samples annealed at $T <$ 600 °C agrees with the XAS experimental findings on the 500 °C, 300 °C, and "as-dep" samples, in which the amount of oxidized copper is so high to hide any clear evidence of the metallic copper presence.

f. Photoluminescence Excitation Analysis. Considerations about the mechanism responsible for the observed PL enhancement can be derived from the PL excitation (PLE) spectra reported in Figure 8, in which the pumping wavelength dependence of the PL emission signal at 1540 nm is analyzed for the sample of the Cu(50−500) group annealed at 500 °C (the best-performing one) and for the corresponding "pure" Er-SiO_2 sample. This last shows some of the typical features related to the Er^{3+} absorption levels, while the Cu-doped one exhibits an excitation profile characterized by a monotonic increase toward the UV, covering the whole visible range. This important modification of the PL excitation spectrum was already observed for systems where Er ions are included in a matrix codoped with metal (Ag, Au) or Si nanoclusters [see ref 13 and references therein].

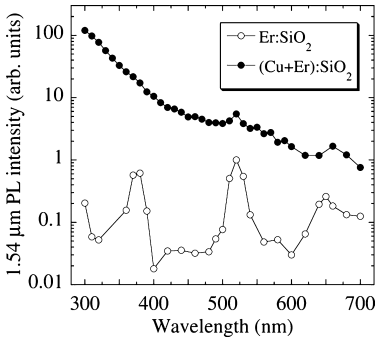

Figure 8. Photoluminescence excitation spectra measured at $\lambda = 1.54$ μm for the sample Cu(50−500) annealed 1 h in air at $T = 500$ °C and for the equivalent "pure" Er:SiO_2 sample after the same annealing treatment. Er ion optical pumping was carried out using a 150-mW Xe lamp coupled with a monochromator. Intensity scale has been calibrated by the photoluminescence measurements performed under the 488.0 nm Ar laser excitation.

DISCUSSION

The presence of Cu atoms inside the Er-SiO_2 sample induces the opening of a new Er excitation channel, triggered by the metal sensitizer, which efficiently absorbs light and promotes a consequent energy-transfer mechanism to the rare-earth ion. The monotonous PLE spectral profile for the codoped system, with just some hints of the resonant rare-earth absorption lines (Figure 8), clearly shows that the system is now able to absorb energy at all of the wavelengths and to transfer it to the rare-earth ion. Moreover, the absence of a significant enhancement of the characteristics resonant rare-earth absorption lines confirms that in our samples the energy-transfer mechanism is not related to the increase of the local electric field owing to a possible plasmon activity of metal particles in the nanometer range of size, as instead supposed by some authors,[56−59] but it is realized by subnanometric copper structures (less than about one hundred of atoms). This is confirmed by the structural and optical analyses, for which the energy-transfer activity starts to disappear when copper particles are of size as large as 1−2 nm or more. As far as the electronic structure of the metallic aggregate is concerned, if compared to the bulk metallic behavior a subnanometric molecular-type cluster undergoes an aperture of the gap between the lowest unoccupied molecular orbital and the highest occupied one, thus showing an electronic structure that seems to be optimal for the transfer of energy to the rare-earth.[13] From a different but equivalent point of view, i.e. by considering a possible band structure, a quantized level structure of the conduction band - with levels grouped into an electronic shell structure - is expected to play an important role at ordinary temperatures only for sufficiently small cluster size: in the case of copper at RT, the Kubo criterion stands that for aggregates formed by a number of atoms $N_{Cu} < 420$, namely for particles having size less than 1.8 nm, the mean level spacing among electronic levels near the

dx.doi.org/10.1021/jp306487a | J. Phys. Chem. C 2012, 116, 21001−21011

Fermi energy is larger than the thermal energy ($E_{thermal} \approx 0.025$ eV at RT).[60] For other elements, this critical size differs no more that 30%, suggesting the possibility that, if the energy-transfer to erbium is mainly allowed by the particular electronic structure of its neighbor subnanometric metallic aggregates, then this process could be independent of the kind of metal.

It is also important to note that in the case of very small Cu nanoparticles (less than 1−2 nm) the interband transitions induce a strong damping and broadening of the SPR band because the energy of the collective oscillation state lies in a quite continuous electron energy region (formed by the one-electron d−sp transition states): as a consequence, the oscillator strength of the transition between the ground state and the surface plasmon collective oscillation one is spread over a wide spectral range.[27] This behavior is present also in the case of Au and Ag small particles, even if less marked than for Cu. As a matter of fact, it could be possible that the wide range of allowed surface plasmon energies provides the way to the dopant atoms to easily transfer the right energy to rare-earth ions. Both these peculiarities of very small aggregates are not strongly dependent on the kind of metallic atoms. Moreover, the similarity between the PLE spectrum features in our case (Cu acting as sensitizers) and in the case of different sensitizers again suggests that for a metallic dopant the aggregates dimension instead of the kind of atom involved could be the main responsible for the sensitization.

Taking into account the observed behavior with the annealing temperature for the intensity and the lifetime of the Er emission at 1.54 μm, and the structure analyses obtained by XAS and Raman spectroscopy, we can try to spread light on the mechanism and the nature of the Cu-related sensitizers. Under cw laser excitation and in low pumping power regime, the 1.54 μm PL intensity for the Er ions is proportional to

$$I_{PL} \propto \sigma \Phi N_{Er} \frac{\tau}{\tau_{rad}} \tag{3}$$

where Φ is the photon flux of the light source, N_{Er} the concentration of optically active Er ions, τ and τ_{rad} are respectively the excited state and the pure radiative lifetime for the $^4I_{13/2} \rightarrow {}^4I_{15/2}$ transition, and σ is the Er ion excitation cross section, with a specific dependence to the pumping wavelength. In the case of an indirect Er excitation process mediated by sensitizing species, the latter term is a peculiar parameter of the system that musts take into account the interaction of the sensitizer with the photon source and the following energy-transfer mechanism to the emitting rare-earth ion. As proposed in refs 61 and 62, we can define an effective cross section σ_{eff}:

$$\sigma_{eff} = \sigma_{sens} N_{sens} \Lambda \frac{\tau_{sens}}{\tau_{tr}} \tag{4}$$

where σ_{sens} and N_{sens} are respectively the excitation cross section and the concentration of the sensitizer, Λ is the Er-sensitizer interaction volume (so that $N_{sens}\Lambda$ is the average number of sensitizing agents surrounding each interacting Er ion), and the ratio between the sensitizer lifetime τ_{sens} (namely the lifetime for the sensitizer energy state involved in the energy-transfer process) and the τ_{tr} energy-transfer time determines the efficiency of the energy-transfer process.

Starting from the measured Er PL intensity and lifetime at a specific Φ, for the synthesized samples, we can define and evaluate the I_{PL}/τ ratio. In Figure 9 we can observe the trend of this parameter with the annealing temperature for each series. In principle, as reported for Er-doped silica,[20,63] at least in the region of full activation of the Er luminescence properties (400−800 °C), the N_{Er} might be constant at an intrinsic value for each series, so the I_{PL}/τ figure-of-merit trend must be totally determined by the annealing temperature dependence of the σ_{eff} cross section.

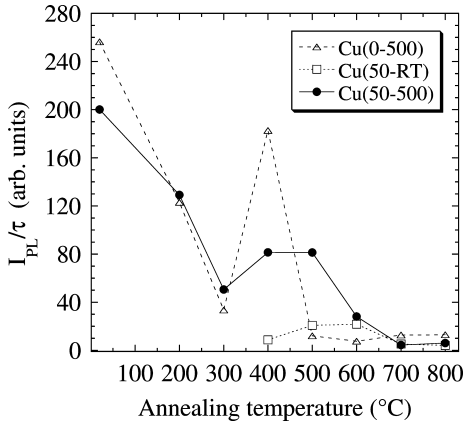

Figure 9. Value of the figure of merit I/τ for the three (Cu+Er):SiO_2 systems, as a function of the temperature of the postsynthesis annealing (1 h in air). λ_{exc} = 488.0 nm. P = 25 mw. All lines are a guide to the eye. Relative uncertainties are around 10%.

In a first approximation, we can consider the intrinsic photophysical parameters characterizing the sensitizing species (σ_{sens} and τ_{sens}) and its interaction with the rare-earth ions (Λ and τ_{tr}) as independent from the synthesis condition. As a consequence, the I_{PL}/τ behavior mainly reflects the variation of the Cu-related sensitizer population N_{sens}, considering that the heating treatment promotes the metal nucleation and growth phenomena with the appearance of larger and larger aggregates as the temperature is raised. Then we try to give account for the trends observed as a function of the annealing temperature, referring to previous studies on Er and metal codoped glasses reported in refs 11, 13, and 39 that investigated the influence of metal clustering on the effectiveness of the Er emission enhancement mechanism.

As evidenced even in these works, the local maximum for annealing temperature in the 400−600 °C range that characterizes the spectra of Figures 3 and 9 can be related to the maximization of the number of Cu-based sensitizing agents as a result of the progressive metal clusterization. Anyways, in the case of the samples synthesized by deposition at 500 °C, the Cu aggregates formation is reasonably started during the deposition itself, originating a strong energy-transfer that allows a very high PL intensity signal even before the annealing treatment (the PL signal is not present in the "pure" Er:SiO_2 systems).

On the basis of our experimental findings, a possible picture of the structural evolution of the different samples can be proposed by considering that, depending on the parameters synthesis, the film characteristics can be different for deposition at different temperatures and with or without a contemporary ion bombardment, as explained by the structure-zone models:[19] (a) for depositions at 500 °C the atoms diffusion at the instantaneous surface of the growing film is increased if compared to RT depositions and (b) depositions with ion bombardment are characterized by a more dense structure. The samples of the groups Cu(0−500 °C) and Cu(50−500 °C) show a PL activity in the as-deposited samples (see Figure 2) due to the formation during deposition of some Cu aggregates

dx.doi.org/10.1021/jp306487a | J. Phys. Chem. C 2012, 116, 21001−21011

of few atoms (nucleation of cluster "seeds"): this is allowed by the increase of the surface diffusion of Cu in a hot growing sample. During the annealing in air at low temperatures (T less than 400 °C), the oxidizing environment causes these small aggregates to oxidize, inducing a decrease of the PL activity. For higher annealing temperatures, the increase of the dopant diffusion coefficient drives the system to favor the aggregation of Cu atoms instead of their oxidation, as expected:[13,28] this causes a new increase of the PL emission. At the highest annealing temperatures the Cu sensitizations decrease abruptly due to the strong precipitation of Cu atoms induced by the marked diffusion and coarsening. The local maximum of the PL emission is much pronounced in the Cu(50−500) (see Figure 2) because here the film structure is much more dense due to the ion bombardment during film growth: this limits the Cu diffusion and the consequent coarsening mechanisms, allowing the Cu aggregates to grow in size but a slower rate. In the Cu(50-RT) sample the absence of the cluster seeds after the RT deposition and the more dense structure due to the ion bombardment make difficult the diffusion and aggregation of Cu atoms: as a consequence, the formation of aggregates of the right size for the sensitization takes place only for annealing temperatures higher than for the other two sample groups. Actually, a contemporary use of different energetic treatments during and after deposition seems to allow a better control of the aggregate formation and dimension, with the aim at optimizing the λ = 1.54 μm PL activity.

CONCLUSIONS

The 1.54 μm Er^{3+} photoluminescence emission has been investigated in Cu-doped Er:SiO_2 films, synthesized by multisource radiofrequency magnetron sputtering with or without additional energy treatment during and after synthesis. Several codoped samples showed a 1.54 μm emission intensity stronger than that in the corresponding "pure" Er:SiO_2 ones prepared under the same synthesis conditions, particularly after postannealing in low temperature regime (T < 700 °C). The enhancement of the 1.54 μm photoluminescence emission has been observed depending on the temperature of the postdeposition annealing. The thermal treatment temperature influences the copper aggregates formation and at the same time the energy-transfer mechanisms to the emitting erbium ions, which are strongly dependent on the cluster size and more efficient in the first stage of the particles formation (size less than 1 nm). PL enhancement due to the copper sensitizers is not related to the presence of a well-defined and clearly visible surface plasmon resonance of metal clusters: on the contrary, a marked reduction of the energy-transfer mechanism efficiency is observed when the surface plasmon resonance is detected in the optical absorption spectra. The copper aggregates formation after the postsynthesis annealing is influenced also by the different energetic treatments undergone by the film during its growth, with clear consequences from the point of view of the film PL properties. The characteristic broadband photoluminescence excitation shown by the Cu-doped Er:SiO_2 system is similar to that observed for Er:SiO_2 systems doped with other metals (also when synthesized by other techniques). This suggests the interesting possibility that the main energy-transfer mechanism in the metal-doped Er:SiO_2 system could be simply related to the very small size (approximately less than 1−2 nm) of the dopant aggregates, in particular to their peculiar electronic properties, defined in relation to the properties of bulk conductors as "quantum size effects" and thus not strictly depending on the aggregate composition. Work is in progress to test this daring hypothesis by the versatility of the multisource radiofrequency sputtering deposition technique, which easily allows the dopant atoms of the Er:SiO_2 starting system to be changed.

AUTHOR INFORMATION

Corresponding Author

*E-mail: cattaruz@unive.it.

Notes

The authors declare no competing financial interest.

REFERENCES

(1) Garrido, B.; García, C.; Seo, S.-Y.; Pellegrino, P.; Navarro-Urrios, D.; Daldosso, N.; Pavesi, L.; Gourbilleau, F.; Rizk, R. *Phys. Rev. B* **2007**, *76*, 245308.
(2) Snoeks, E.; van den Hoven, G. N.; Polman, A.; Hendriksen, B.; Diemeer, M. B. J.; Priolo, F. *J. Opt. Soc. Am. B* **1995**, *12*, 1468.
(3) Auzel, F. *Phys. Rev. B* **1976**, *13*, 2809.
(4) Strohhöfer, C.; Polman, A. *Opt. Mater.* **2003**, *21*, 705.
(5) Fujii, M.; Yoshida, M.; Kanzawa, Y.; Hayashi, S.; Yamamoto, K. *Appl. Phys. Lett.* **1997**, *71*, 1198.
(6) Kik, P. G.; Polman, A. *J. Appl. Phys.* **2000**, *88*, 1992.
(7) Pacifici, D.; Franzò, G.; Priolo, F.; Iacona, F.; Dal Negro, L. *Phys. Rev. B* **2003**, *67*, 245301.
(8) Strohhöfer, C.; Polman, A. *Appl. Phys. Lett.* **2002**, *81*, 1414.
(9) Mattarelli, M.; Montagna, M.; Vishnubhatla, K.; Chiasera, A.; Ferrari, M.; Righini, G. C. *Phys. Rev. B* **2007**, *75*, 125102.
(10) Mazzoldi, P.; Padovani, S.; Enrichi, F.; Mattei, M.; Trave, E.; Guglielmi, M.; Martucci, A.; Battaglin, G.; Cattaruzza, E.; Gonella, F.; Maurizio, C. *SPIE Proc.* **2004**, *5451*, 311.
(11) Trave, E.; Mattei, G.; Mazzoldi, P.; Pellegrini, G.; Scian, C.; Maurizio, C.; Battaglin, G. *Appl. Phys. Lett.* **2006**, *89*, 151121.
(12) Watekar, P. R.; Seongmin, J.; Won-Taek, H. *Colloids Surf., A* **2008**, *313−314*, 492.
(13) Maurizio, C.; Trave, E.; Perotto, G.; Bello, V.; Pasqualini, D.; Mazzoldi, P.; Battaglin, G.; Cesca, T.; Scian, C.; Mattei, G. *Phys. Rev. B* **2011**, *83*, 195430.
(14) Ferrari, M.; Righini, G. C. Rare-earth-doped glasses for integrated optical amplifiers. *Physics and Chemistry of Rare-Earth Ions Doped Glasses*; Materials Science Foundations (monograph series); Hussain, N. S., Santos, J. D., Eds.; Trans Tech Publishers (ttp): Switzerland, 2008; Vols. *46−47*, Chapter 3.
(15) Mooradian, A. *Phys. Rev. Lett.* **1969**, *22*, 185.
(16) Boyd, G. T.; Yu, Z. H.; Shen, Y. R. *Phys. Rev. B* **1986**, *33*, 7923.
(17) Yeshchenko, O. A.; Dmitruk, I. M.; Dmytruk, A. M.; Alexeenko, A. A. *Mater. Sci. Eng., B* **2007**, *137*, 247.
(18) Borsella, E.; Dal Vecchio, A.; Garcìa, M. A.; Sada, C.; Gonella, F.; Polloni, R.; Quaranta, A.; van Wilderen, L. J. G. W. *J. Appl. Phys.* **2002**, *91*, 90.
(19) Thornton, J. A. *J. Vac. Sci. Technol. A* **1986**, *4*, 3059.
(20) Cattaruzza, E.; Battaglin, G.; Trave, E.; Visentin, F. *Thin Solid Films* **2011**, *519*, 5376.
(21) Di Cicco, A.; Aquilanti, G.; Minicucci, M.; Principi, E.; Novello, N.; Cognigni, A.; Olivi, L. *J. Phys.: Conf. Ser.* **2009**, *190*, 012043.
(22) Snoeks, E.; Kik, P. G.; Polman, A. *Opt. Mater.* **1996**, *5*, 159.
(23) Maurizio, C.; Iacona, F.; D'Acapito, F.; Franzò, G.; Priolo, F. *Phys. Rev. B* **2006**, *74*, 205428.
(24) Cattaruzza, E.; Battaglin, G.; Visentin, F.; Trave, E. *J. Non-Cryst. Solids* **2009**, *355*, 1128.
(25) Kreibig, U.; Vollmer, M. *Optical Properties of Metal Cluster*; Springer Series in Materials Science; Springer: Berlin, 1995; Vol. *25*.
(26) Lermé, J.; Palpant, B.; Cottancin, E.; Pellarin, M.; Prével, B.; Vialle, J. L.; Broyer, M. *Phys. Rev. B* **1999**, *60*, 16151.
(27) Celep, G.; Cottancin, E.; Lermé, J.; Pellarin, M.; Arnaud, L.; Huntzinger, J. R.; Vialle, J. J.; Broyer, M.; Palpant, B.; Boisron, O.; Mélinon, P. *Phys. Rev. B* **2004**, *70*, 165409.

(28) Miotello, A.; De Marchi, G.; Mattei, G.; Mazzoldi, P.; Sada, C. *Phys. Rev. B* **2001**, *63*, 075409.
(29) Battaglin, G.; Cattaruzza, E.; Gonella, F.; Polloni, R.; D'Acapito, F.; Colonna, S.; Mattei, G.; Maurizio, C.; Mazzoldi, P.; Padovani, S.; Sada, C.; Quaranta, A.; Longo, A. *Nucl. Instrum. Methods B* **2003**, *200*, 185.
(30) Blondeau, J.-P.; Pellerin, S.; Vial, V.; Dzierżęga, K.; Pellerin, N.; Andreazza-Vignolle, C. *J. Cryst. Growth* **2008**, *311*, 172.
(31) Cattaruzza, E.; Battaglin, G.; Canton, P.; Finotto, T.; Sada, C. *Mater. Sci. Eng., C* **2006**, *26*, 1092.
(32) Johnson, P. B.; Christy, R. W. *Phys. Rev. B* **1972**, *6*, 4370.
(33) http://www.ioffe.ru/SVA/NSM/nk/Metals/Gif/cu.gif
(34) Cottancin, E.; Celep, G.; Lermé, J.; Pellarin, M.; Huntzinger, J. R.; Vialle, M.; Broyer, J. L. *Theor. Chem. Acc.* **2006**, *116*, 514.
(35) Cattaruzza, E.; Battaglin, G.; Canton, P.; Sada, C. *J. Non-Cryst. Solids* **2005**, *351*, 1932.
(36) Sun, H.-B.; Juodkazis, S.; Watanabe, M.; Matsuo, S.; Misawa, H.; Nishii, J. *J. Phys. Chem. B* **2000**, *104*, 3450.
(37) Priolo, F.; Franzò, G.; Pacifici, D.; Vinciguerra, V.; Iacona, F.; Irrera, A. *J. Appl. Phys.* **2001**, *89*, 264.
(38) Miritello, M.; Lo Savio, R.; Iacona, F.; Franzò, G.; Irrera, A.; Piro, A. M.; Bongiorno, C.; Priolo, F. *Adv. Mater.* **2007**, *19*, 1582.
(39) Martucci, A.; de Nuntis, M.; Ribaudo, A.; Guglielmi, M.; Padovani, S.; Enrichi, F.; Mattei, G.; Mazzoldi, P.; Sada, C.; Trave, E.; Battaglin, G.; Gonella, F.; Borsella, E.; Falconieri, M.; Patrini, M.; Fick, J. *Appl. Phys. A: Mater. Sci. Process.* **2004**, *80*, 557.
(40) Wojdak, M.; Klik, M.; Forcales, M.; Gusev, O. B.; Gregorkiewicz, T.; Pacifici, D.; Franzò, G.; Priolo, F.; Iacona, F. *Phys. Rev. B* **2004**, *69*, 233315.
(41) Witkowska, A.; Di Cicco, A.; Principi, E. *Phys. Rev. B* **2007**, *76*, 104110.
(42) Duval, E.; Boukenter, A.; Champagnon, B. *Phys. Rev. Lett.* **1986**, *56*, 2052.
(43) Malinovsky, V. K.; Novikov, V. N.; Sokolov, A. P.; Dodonov, V. G. *Solid State Commun.* **1998**, *67*, 725.
(44) Mariotto, G.; Montagna, M.; Viliani, G.; Duval, E.; Lefrant, S.; Rzepka, E.; Mai, C. *Europhys. Lett.* **1998**, *6*, 239.
(45) Montagna, M.; Dusi, R. *Phys. Rev. B* **1995**, *52*, 10080.
(46) Ivanda, M.; Babocsi, K.; Dem, C.; Schmitt, M.; Montagna, M.; Kiefer, W. *Phys. Rev. B* **2003**, *67*, 235329.
(47) Duval, E.; Portes, H.; Saviot, L.; Fuji, M.; Sumitomo, K.; Hayashi, S. *Phys. Rev. B* **2001**, *63*, 075405.
(48) Lipinska-Kalita, K. E.; Krol, D. M.; Hemley, R. J.; Mariotto, G.; Kalita, P. E.; Ohki, Y. *J. Appl. Phys.* **2005**, *98*, 054301.
(49) Sirotkin, S.; Cottancin, E.; Saviot, L.; Bernstein, E.; Mermet, A. *Phys. Rev. B* **2012**, *85*, 205435.
(50) Quaranta, A.; Rahman, A.; Mariotto, G.; Maurizio, C.; Trave, E.; Gonella, F.; Cattaruzza, E.; Ghibaudo, E.; Broquin, J. E. *J. Phys. Chem. C* **2012**, *116*, 3757.
(51) Lipinska-Kalita, K. E.; Mariotto, G.; Zanghellini, E. *Phil. Mag. B* **1995**, *71*, 547.
(52) Ceccato, R; Dal Maschio, R.; Gialanella, S.; Mariotto, G; Montagna, M.; Rossi, F.; Ferrari, M.; Lipinska-Kalita, K. E.; Ohki, Y. *J. Appl. Phys.* **2001**, *90*, 2522.
(53) Ceccato, R.; Dal Maschio, R.; Ferrari, M.; Gialanella, S.; Lipinska-Kalita, K. E.; Mariotto, G.; Montagna, M.; Ohki, Y.; Rossi, F. *J. Raman Spectrosc.* **2001**, *32*, 643.
(54) Ivanda, M.; Hohl, A.; Montagna, M.; Mariotto, G.; Ferrari, M.; Crnjak Orel, Z.; Turkovic, A.; Furic, K. *J. Raman Spectrosc.* **2006**, *37*, 161.
(55) Foote, K. G. *J. Acoust. Soc. Am.* **1982**, *71*, 742.
(56) Malta, O. L.; Santa-Cruz, P. A.; de Sà, G. F.; Auzel, F. *J. Lumin.* **1985**, *33*, 261.
(57) Hayakawa, T.; Selvan, S .T.; Nogami, M. *Appl. Phys. Lett.* **1999**, *74*, 1513.
(58) Selvan, S. T.; Hayakawa, T.; Nogami, M. *J. Phys. Chem. B* **1999**, *103*, 7064.
(59) Fukushima, M.; Managaki, N.; Fujii, M.; Yanagi, H.; Hayashi, S. *J. Appl. Phys.* **2005**, *98*, 024316.
(60) Schaaff, T. G.; Shafigullin, M. N.; Khoury, J. T.; Vezmar, I.; Whetten, R. L.; Cullen, W. G.; First, P. N.; Gutiérrez-Wing, C.; Ascensio, J.; Jose-Yacamán, M. J. *J. Phys. Chem. B* **1997**, *101*, 7885.
(61) Franzò, G.; Vinciguerra, V.; Priolo, F. *Appl. Phys. A: Mater. Sci. Process.* **1999**, *69*, 3.
(62) Kenyon, A. J.; Chryssou, C. E.; Pitt, C. W.; Shimizu-Iwayama, T.; Hole, D. E.; Sharma, N.; Humphreys, C. J. *J. Appl. Phys.* **2002**, *91*, 367.
(63) Polman, A. *J. Appl. Phys.* **1997**, *82*, 1.